Shock-Structure Formation in Circular and Non-Circular Sonic Jets at Underexpanded Conditions

T. Thangaraj[1], T. Jana[2], M. Kaushik[3†] and T. Subramanian[4]

[1, 3] *School of Aeronautical Sciences, Hindustan Institute of Technology and Science, Chennai, Tamilnadu, 603103, India*

[2] *Department of Aerospace Engineering, JAIN (Deemed-to-be University), Bangalore, Karnataka, 560069, India*

[3] *Department of Aerospace Engineering, Indian Institute of Technology Kharagpur, Kharagpur, West Bengal, 721302, India*

[4] *Department of Aerospace Engineering, Madras Institute of Technology, Chennai, Tamil Nadu, 600044, India*

†*Corresponding Author Email: mkaushik@aero.iitkgp.ac.in*

ABSTRACT

The generation of shock waves and their repercussions in high-speed vehicles are inevitable. Particularly, the hot plume from the aircraft exhaust ejecting at a high speed, as well as the emitted aeroacoustic noise, have several consequences. Besides, the occurrence of the supersonic core length and the emission of high screech noise are mostly due to the shock cells, prevailing in high-speed jets. Therefore, understanding the shock cell structures developed at the exit of aircraft or rocket nozzles is vital in improving mixing and thereby the noise characteristics. Essentially, non-circular nozzle shapes are well known for enhancing entrainment characteristics and mitigating the noise due to their differential spreading over the nozzle's perimeter. The current study examines the shock structures of circular, elliptic, and square jets at various sonic underexpansion levels. In this investigation, the nozzle geometries are considered to have the same exit area. The Nozzle Pressure Ratio (NPR) was adjusted to 3, 4, and 5 to achieve moderate and highly underexpansion conditions. The shadowgraph visualization method is used to study the development of shock cells from axisymmetric and asymmetric nozzles. It is interesting to observe that the incident and reflected shock structures exist only at moderate and high underexpansion levels. Besides, the elliptic and the square jets have distinctive flow patterns along their different axis planes. The intercepting shock appears on the elliptic jet in the minor axis rather than the major axis direction. The curvature of the intercepting shock wave was found to be greater for the elliptic jet than that for the circular jet. In addition, the square jet in the symmetry plane diverges from the jet centerline, but the jet in the diagonal direction converges. Moreover, the estimated shock cell lengths using shadowgraph images were compared to a theoretical model where the experimentally obtained results are in good agreement with the theoretical values.

Keywords: Non-circular nozzle; Sonic underexpansion; Shadowgraph visualization; Shock cell structures; Mach disk.

NOMENCLATURE

D_{eq}	equivalent nozzle exit diameter	Y	distance along the major-axis and the symmetry plane for elliptic nozzle and square nozzle, respectively
L_s	Shock cell length		
M_j	jet Mach number		
NPR	Nozzle Pressure Ratio	Z	distance along the minor-axis and the diagonal plane for elliptic nozzle and square nozzle, respectively
P_0	settling chamber pressure		
P_{atm}	ambient pressure or back pressure		
X	distance in the streamwise direction	γ	specific heat ratio

1. INTRODUCTION

High-pressure gaseous jets ejected from the nozzles are governed by the complex flow structure. Understanding these structures is critical for analyzing aerodynamic mixing and aeroacoustic noise behavior, specifically for aircraft and rocket nozzles. According to the requirement, convergent or convergent-divergent types of nozzles are utilized in the aerospace industry. In a convergent nozzle, the possible expansion processes are correct-expansion and underexpansion based on the operating nozzle pressure ratio. On the other hand, the convergent-divergent nozzle is associated with three different expansion processes: overexpansion, correct-expansion, and underexpansion. For the convergent nozzle, the flow is correctly-expanded at the condition where the ratio of exit pressure (p_e) to ambient pressure (p_a) equals unity ($p_e/p_a = 1$). When the pressure ratio (p_e/p_a) exceeds one, underexpansion occurs and pressure equilibrium is obtained outside the nozzle, where the shock cell structures dominate the jet core. Essentially, the mass discharge at the nozzle outlet increases with the inlet pressure until the mass flow attains its maximum value at sonic conditions. Further increase in the inlet pressure has no additional impact on the mass flow as the flow is choked at that condition (Kaushik 2019). The flow characteristics of an underexpanded axisymmetric jet, i.e., structures of shock waves, the expansion fan, and the development of the shear layer are well documented in the literature (Adamson and Nicholls 1959). Moreover, the development of the Mach disc in a highly underexpanded circular jet is comprehended (Addy 1981). There are several studies that aim to modify the circular geometry using grooves or tabs. When grooves are employed at the exit of a circular nozzle, differential shock cell formations in the nearfield region are observed. This is due to the local shock waves generated by the grooves (Ilakkiya and Sridhar 2018). The presence of tabs in a supersonic jet, on the other hand, causes the jet to split along the tab orientation, meanwhile, the jet merges in the direction normal to the tab (Jana and Kaushik 2021). Besides, the nozzles having different shapes other than an axisymmetric nozzle may have different flow topologies in different plane directions (Lee *et al.* 2012). Keeping this in mind, the flow properties of elliptic and square jets are particularly considered for the current study.

An elliptic nozzle has a curvature that varies azimuthally around its perimeter, resulting in differential spreading. As a result of this phenomenon, axes switch in the downstream location, which is referred to as axis switching. The enhanced entrainment of elliptic jets over circular jets is essentially due to this axis-switching mechanism. The plane containing the major axis is associated with the smallest radius of curvature; whereas, the largest radius of curvature is connected with the minor axis plane. Note that, the portion of the major axis plane moves at a faster rate than the plane containing the minor axis (Austin and Ho 1992). Consequently, the elliptic jet experiences streamwise cross-sectional deformation, which leads to the jet axes switching in the near stream location (Gutmark and Ho 1986). It goes through this periodic process until it takes on a symmetrical form. Ho and Gutmark have conducted an experimental study on the spreading properties of an elliptic jet in the region of subsonic flow (Ho and Gutmark 1987). It was discovered that the mass entrainment rate was significantly higher than that of an axisymmetric jet. An elliptic nozzle experiences an axis-switch as a result of the non-uniform distribution of vortices along its perimeter, which also increases the rate of entrainment. Schadow *et al.* (1989) performed an experimental study on the mixing behaviors of circular and elliptic jets in the domains of subsonic and sonic flows. The Schlieren method was utilized to observe the shock structures that prevail in the sonic underexpanded jet. The axis switching location was found to be dependent on the jet exit velocity and the nozzle aspect ratio. Moreover, the elliptic jet exhibits an asymmetric pattern of compression and expansion waves created in the jet core. A systematic study of an oval nozzle at sonic underexpanded conditions was undertaken by (Rajakuperan and Ramaswamy 1998). In this study, they explored the influence of pressure ratio and aspect ratio on mixing characteristics. The Pitot pressure measurements and shadowgraph system were implemented to acquire the data. It can be noted that, at low aspect ratios, the jet structure is similar to that of an axisymmetric jet. However, with a large aspect ratio, the jet structure differs along major and minor axis directions. At a high aspect ratio, the jet structure in the major axis direction resembles the circular jet, with prominent barrel and reflected shocks. However, the barrel shock is not evident along the minor axis direction. Moreover, when the nozzle pressure ratio is increased, the jet spread rate is also increased. (Verma and Rathakrishnan 2001) performed experiments to visualize the shock cell structures of an elliptic slot at moderately and highly underexpanded jets. It was observed that the shock cell patterns developed in both planes are different. This is due to the differential growth rate of the mixing region along both axes. The minor axis direction had a faster growth rate than the major axis direction. Menon and Skews (2010) investigated the shock cell patterns of various non-circular geometries at sonic underexpanded conditions. They compared the development of shock cells between the jets ejecting from the elliptic nozzle and the slot. At a nozzle pressure ratio of 2 and 3, the nozzle aspect ratio was varied as 1, 2, and 4. It was observed that both the elliptic nozzle and the slot have identical jet structures. It was also noted that, along the major axis plane, the incident shock originates right at the nozzle outlet. In contrast, the incident shock generates at some downstream distance along the minor axis plane.

Furthermore, the incident shock is not visible at any pressure ratio when the aspect ratio is greater than two. Mitchell *et al.* (2013) used the Schlieren and PIV techniques to perform both qualitative and quantitative evaluations on a contoured elliptic jet. The measurements were carried out with an elliptic nozzle of aspect ratio 2 at various underexpansion levels. The axis switching phenome-non was detected in the PIV measurements for all pressure ratios. Moreover, as the nozzle pressure ratio is increased, the strength of axis switching rises. The existence of a Mach disc, triple point, and slip line was seen in the Schlieren pictures at nozzle pressure ratios larger than 2.6. In addition, vortex bifurcation was detected at the highest pressure ratio. Jothi and Srinivasan (2019) studied shock cell topologies with a variety of slot geometry under sonic underexpanded circumstances. They found differential spreading along both the major and minor axes. They have also seen the axis switching behavior, which is prevailing in the downstream region ranging from 3 to 7 times the diameters from the nozzle exit. Furthermore, the width of the shock cell is seen to be higher along the major axis.

On the other hand, because of the addition of flat segments and sharp edges, the square nozzle results an increase in mass entrainment. The jet from the segment with the sharp corners flows more quickly in the axial direction than the jet from the segment with the flat sides (Jiang *et al.* 1999). Due to the non-uniform flow shape from the flat and corner parts, the unique spreading and thereby the axis switches phenomenon is observed at the downstream side. Tsutsumi *et al.* (2006) presented the results of the numerical and experimental study of underexpanded square jets. In that study, they noticed the intercepting and recompression shock waves in the core of the square jet. Both intercepting and recompression shock waves are crucial in the formation of the cross-shaped cross-section. Interestingly, the cross-shaped cross-section becomes stronger as the pressure ratio increases. In addition, several researchers employed three-dimensional visualization techniques to examine the shock structures developed by the square nozzles. Zare-Behtash *et al.* (2008) investigated compressible vortex loops with axisymmetric and asymmetric shapes, including elliptic and square configurations. They conducted quantitative and qualitative measurements to explain the vortex ring instabilities and the existence of shock waves in the vortex loop. In every case, as the flow begins, weak vortices emerge and get stronger, causing azimuthal disturbances in the shear layer. PIV results revealed that the core region of the elliptic vortex loop travels in a transverse direction, whereas the core of the square vortex loop travels in a streamwise manner. The shock waves embedded in the jet core were also seen. The jet boundary shape of square nozzles was examined by Menon and Skews (2010). The jet with a square cross-section at the nozzle exit becomes approximately circular at some downstream

distance. The three-dimensional structure of the jet, which is based on the interaction of reflected shock on the jet boundary, has been noticed. The evolution of three-dimensional structures of the square jet was demonstrated by Zhang *et al.* (2017). The shock wave surface becomes more strong as the nozzle pressure ratio increases. The jet boundary is suppressed by the shock surface formed at the corner section. The jet edge, on the other hand, spreads along the flat edges. As a result of this process, the cross-section of the square jet becomes cross-shaped. The jet boundary is significantly distorted in a highly underexpanded jet, resulting in rapid shear layer growth. The influence of vertices and edges in square shapes contributes to the faster spread of the vortex ring (Jothi and Srinivasan 2019). The employment of tabs or non-circular nozzle geometries weakens the shock cell structures and reduces the shock cell spacing as compared to a circular jet (Tanna 1977; Verma and Rathakrishnan 1998). These phenomena essentially lead to the mitigation of screech tone and shock-associated noise, emitted from the supersonic jet (Jothi and Srinivasan 2013). The recent review paper by Thangaraj *et al.* (Thangaraj *et al.* 2022) beautifully describes the shock cell structure and the underlying mechanism behind the supersonic jet mixing characteristics at different Nozzle Pressure Ratio. They concluded that the asymmetric nozzle alters the shock cell structure and thereby reduces the emission of aeroacoustic noise.

From the aforementioned studies, it is clear that though a substantial amount of work has been done in order to study the mixing behavior of asymmetric jets; however, the analysis of shock cell structures for sonic underexpanded elliptic and square jets has been hardly looked into. Moreover, previous studies on sonic underexpanded jets are mostly concentrated on moderately-underexpanded jets with slot layouts of elliptic geometries. The influence of the nozzle at moderately and highly-underexpanded conditions is seldom documented in the literature. Keeping this in mind, the shock cell structures that prevail in the circular, elliptic, and square jets at various underexpansion levels are investigated in this study. Moderate and high-underexpansion levels are produced by varying the nozzle pressure ratio to 3, 4, and 5. To capture the shock cell structures that developed in the jet core, a shadowgraph system has been used. The shock cell images were recorded in different plane directions for elliptic and square nozzle shapes.

2. EXPERIMENTAL METHODOLOGY

The experiments were carried out at the free jet-testing setup, which has an air supply arrangement and a free jet-testing configuration. The compressor and a storage tank are the main parts of the air supply system. Fig. 1 depicts the components of the jet-test setup, which comprises of gate valve, pressure regulating valve, settling chamber with nozzle fitting provision, pressure gauge, and data collecting system.
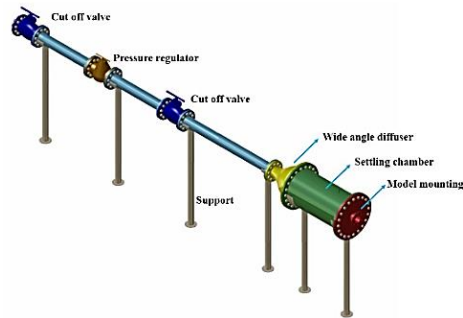
Fig. 1. Schematic view of the free jet-testing setup.

2.1 Air Supply System

The air in the storage tank is compressed using a two-stage reciprocating compressor. The 80 hp 3-phase motor driving the compressor can deliver a discharge pressure up to the level of 150 psi. A cylindrical tank with a capacity of 30,000 liters houses the compressed air. A pressure regulator and gate valve are part of the tunnel control section. The settling chamber assembly and a mixing tube with a 3-inch diameter are attached to the pressure controller.

2.2 Free Jet-Testing Setup

Fig. 2 displays the picture of free jet-testing setup. In the testing facility, the air reservoir is attached to a settling chamber. Particularly, the gate valve, pressure controller, and mixing tube are used to move the pressurized air from the reservoir before it enters the settling chamber. A wide-angle diffuser connects the settling chamber to the mixing tube, and two wire mesh screens are placed behind it to lessen turbulence at the nozzle entry. To help the air settle and come to balance, screens are installed in the settling chamber. The length and the internal diameter of the settling chamber is 600 mm and 300 mm, respectively. A pressure sensor is mounted on the settling chamber to track the pressure within the chamber.

Fig. 2. Photographic view of the free jet-testing setup.

The settling chamber pressure is a governing factor in this inquiry. During a run, by managing the pressure regulator, the settling chamber pressure can be altered. Note that, the nozzle pressure ratio (NPR) is the ratio of the stagnation pressure to the surrounding pressure or back-pressure. The temperature in the settling chamber is kept constant with the ambient temperature. The ambient temperature was essentially consistent throughout the experiment (varied within 0.5°C). The accuracy

of the stagnation pressure measurement is ±0.1%. During each run, the settling chamber's pressure was monitored by the pressure transducer.

2.3 Test Conditions

The current investigation examines the shock cell structures prevailing in the jets, ejected from the circular and non-circular nozzle outlet shapes (elliptic and square) at different sonic underexpanded conditions. The test was carried out at nozzle pressure ratios of 3, 4, and 5, which correspond to moderately and highly underexpanded jet circumstances, respectively. Note that, desired nozzle pressure ratio will be achieved by regulating the pressure level in the settling chamber. The following is the equation that relates the nozzle pressure ratio and the nozzle exit Mach number (Kaushik 2019).

$$NPR = \frac{P_0}{P_{atm}} = \left(1 + \frac{\gamma - 1}{2} M_j^2\right)^{\frac{\gamma}{\gamma - 1}} \qquad (1)$$

$$M_j = \sqrt{\frac{2}{\gamma - 1}\left[\left(\frac{P_0}{P_{atm}}\right)^{\frac{\gamma - 1}{\gamma}} - 1\right]} \qquad (2)$$

In the present investigation, the Shadowgraph methods are utilized to visualize the shock and expansion wave structure in underexpanded sonic jets. It should be noted that the structure of non-circular jets varies around their circumference. Therefore, to obtain an overall picture, photographs are taken in both the major (Y-axis) and minor axis (Z-axis) directions for the elliptic jet. Likewise, for the square jet, images were collected along the symmetry (Y-axis) and diagonal (Z-axis) directions. For the circular jet, the images are collected in one direction since the jet structure is axisymmetric.

2.4 Experimental Models

Stainless steel was utilized to make the test nozzles for this investigation. In Fig. 3, the nozzle geometries taken into consideration in the current work are schematically shown. Elliptic and square forms of non-circular nozzle exit geometries are taken into consideration in the study. Note that, the constant exit area for each nozzle is 314 mm². Accordingly, the equivalent circular nozzle outlet diameter is calculated as 20 mm. Figure 4 shows images of nozzles with square, elliptical and circular geometries. The photographic view of the assembly of these nozzles at the outlet of the settling chamber is shown in Fig. 5.

The Shadowgraph flow visualization is convenient for detecting the density gradient in a flow field (Rathakrishnan 2007). Using this method, shock and expansion wave structures for circular and non-circular sonic jets in various underexpanded states can be seen. The schematic representation of the shadowgraph system is shown in Fig. 6. A 150 mm concave mirror and a Helium light source are included in the shadowgraph system. Using a still camera, pictures of the shock cell architectures were recorded. The mirror has a 1.6 m focal length and λ/6 is the extent of surface finish.
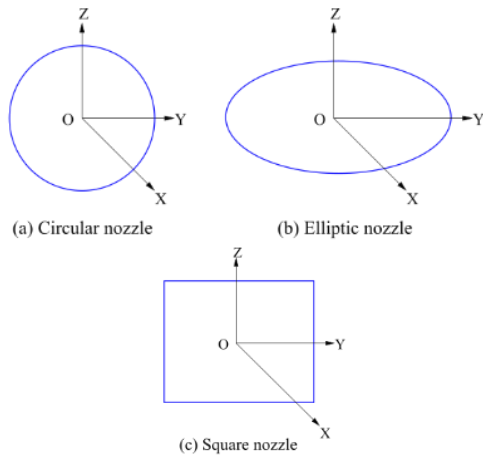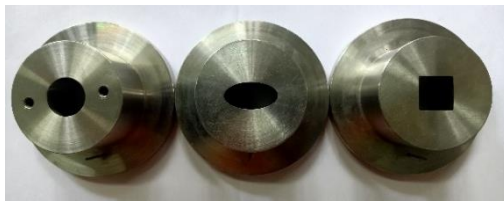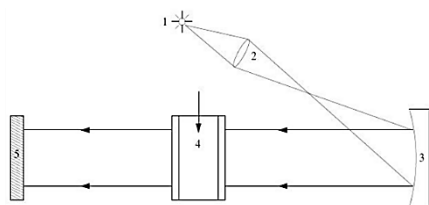
Fig. 3. Schematic views of the nozzle outlet geometries

Fig. 4. Image of the circular, elliptic, and square nozzles.

Fig. 5. Image of the square nozzle attached to the settling chamber.

2.5 Shadowgraph Method

1. Light source   3. Concave mirror   5. Screen
2. Condensing lens 4. Test section

Fig. 6. Schematic representation of the shadowgraph flow visualization system.

3. RESULTS AND DISCUSSION

This section presents shadowgraph images of circular and non-circular jets in order to analyze the shock cell structures prevailing in the jet core. Firstly, the core of the circular jet is analyzed at various nozzle pressure ratios. Following that, the core of elliptic and square jets, captured along the Y- and Z-axes planes, are investigated. Finally, the shock cell lengths for different nozzle geometries are calculated.

3.1 Flow Visualization

The shadowgraph images obtained at various nozzle pressure ratios for the circular jet are provided in Fig. 7. For nozzle pressure ratio 3, the estimated Mach number at the nozzle exit using an isentropic relation is 1.35. At this Mach number, the Prandtl-Meyer expansion waves are formed at the nozzle's lip. The produced expansion waves collide at the jet-axis/centerline, travel back to the jet edge, and then reflect as compression waves. Since the reflection is unlike, the expansion waves incident at the jet edge is reflected as compression waves. The compression waves combine to generate the oblique shock, which is directed towards the jet axis. Subsequently, these opposite side oblique shocks collide at the jet centerline before reflecting from the jet edge as expansion waves. As a result, the first shock cell forms in the jet core. In a similar manner, subsequent shock cell structures develop in the jet core. Here, around six shock-cell structures can be viewed in the jet core.
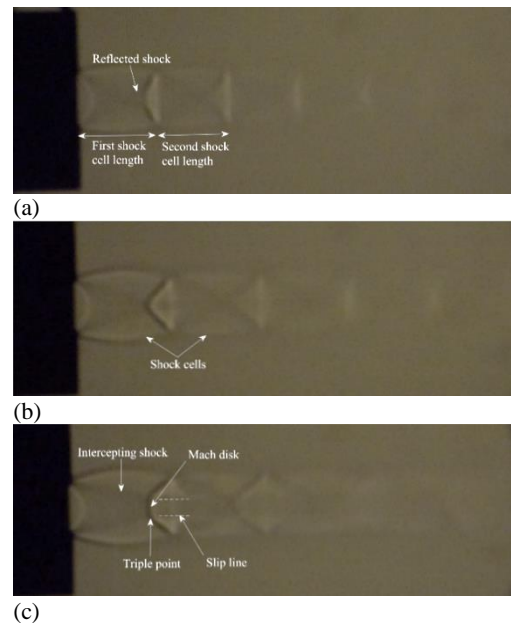

Fig. 7. Shadowgraph views of the circular jet at (a) NPR 3 (b) NPR 4 (c) NPR 5.

In addition, the size of the shock cells decreases continuously along the downstream distance. Notice that, the first two shock cells are prominent, while the following shock cells appear to be hazy. The length of the shock cell, on the other hand, is

directly related to the distance between the nozzle exit plane and the point where two intercepting shocks meet the jet boundary (Fig. 7(a)). Consequently, an increase in the nozzle pressure ratio to 4 leads to an increase in the size of the shock cells. In comparison to the preceding scenario, the number of shock cells that could be accommodated for the same space was decreased as a result of increased shock cell size. At this nozzle pressure ratio, four shock cells were observed in the jet core, as shown in Fig. 7(b). Furthermore, an increase in nozzle pressure ratio to 5 results in Mach disc formation. The Mach disc emerges at the region where the intercepting shocks collide at the jet axis. When the regular reflection transforms into Mach reflection in the shock intersection region, the Mach disc appears. It can be noted that the Mach reflection phenomenon occurs when the flow turning angle across the intercepting shock is larger than the turning angle across the reflected shock. The shock intersection point is transformed into the intersection region during the Mach reflection. In this region Mach stem or Mach disk, triple points, and slip lines were observed, as exhibited in Fig. 7(c). At nozzle pressure ratio 5, four shock cells were seen. For this case, the shock cell structures are greater in size than that in earlier situations. Notice that, Only the first two shock cells are clearly visible for the nozzle pressure ratio 5.

Figure 8 shows the shadowgraph images of the elliptic jet at different pressure ratios. The elliptic jet displays no intercepting shock along the Y-axis (major axis), however, the intercepting shock is noticeable along the Z-axis (minor axis). At nozzle pressure ratio 3, the opposite side of intercepting shock waves reflects during the regular reflection (Fig. 8(a)). When the nozzle pressure ratio (NPR) increases to 4, the development of Mach reflection occurs at the intersection of the intercepting shock waves. The Mach disk looks to be quite small in size, as shown in Fig. 8(b). The wave pattern for the elliptic jet in the direction along minor axis appears to be identical to that of the circular jet. However, the curvature of the intercepting shock wave in an elliptic jet is substantially greater than that for the circular jet. The size of the shock cells, as well as, the Mach disk height is higher at a NPR of 5. The width of the Mach disk for the elliptic jet is different along both the minor and major axes (Fig. 8(c)). The Mach disk width is higher along the major axis. Furthermore, the width of the reflected shock at the interaction region is greater along the major axis, when compared with the minor axis. This is due to the fact that the size of the jet boundary is higher along the major axis than that along the minor axis.

The jet structure of a square jet differs noticeably from the circular jet at a nozzle pressure ratio 3, as observed in Fig. 9. It should be noticed that the oblique shock appears at the nozzle exit when viewed along the Y-axis direction, however, it appears little away from the nozzle outlet plane when viewed along the Z-axis direction (Fig. 9(a)). Surprisingly, the oblique shock created at the nozzle exit is not caused by reflected expansion waves
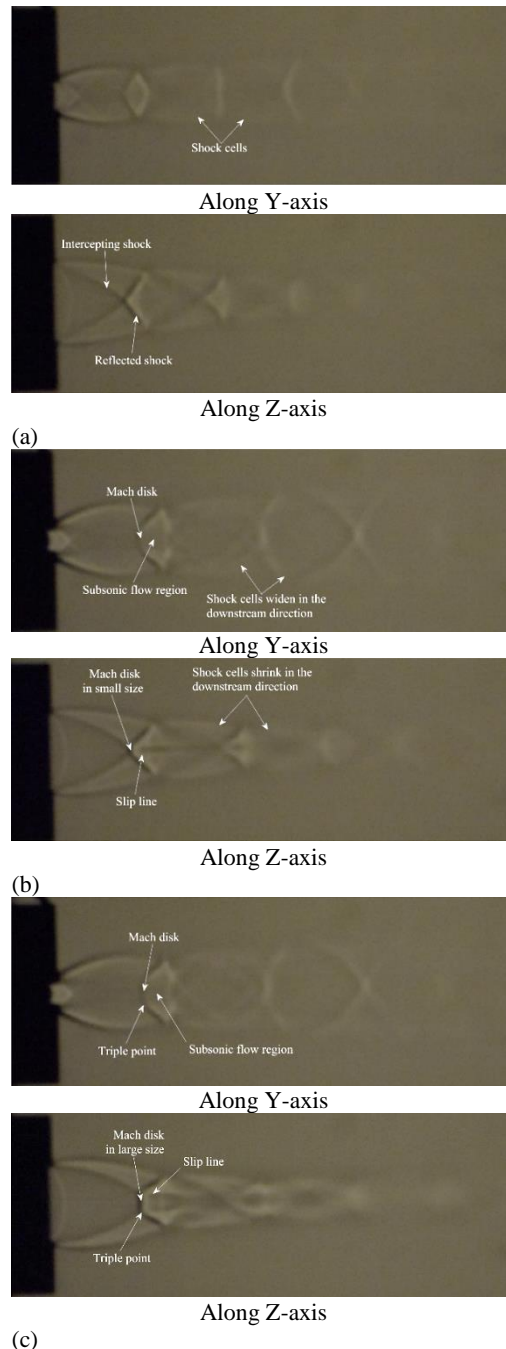

Along Y-axis

Along Z-axis

(a)

Along Y-axis

Along Z-axis

(b)

Along Y-axis

Along Z-axis

(c)

Fig. 8. Shadowgraph views of the elliptic jet at (a) NPR 3 (b) NPR 4 (c) NPR 5.

from the jet boundary; rather, it's a recompression shock that forms at the lip of the square nozzle. The generation of recompression shock can be explained as follows; the expansion waves emerge from the edges of the square nozzle and their interaction at the corner region causes the flow to become overexpanded. In the overexpanded region, the static pressure drops below the ambient level. Hence, in order to achieve the ambient pressure, the recompression shock is generated. In addition, along the Y-axis direction, another recompression shock wave is observed at some downstream

location. The overexpanded flow from the corner region grows in the downstream direction and collides with the adjacent region. This process yields a second recompression shock wave along the Y-axis direction. Moreover, the intercepting shocks are observed in both symmetry and diagonal orientations. These intercepting shock waves are formed by the reflection of expansion waves from the jet boundary. Furthermore, the reflection of the recompression shock wave is observed along both the symmetry and the diagonal directions. Notice that, the shape of a square j*et al*ong both the Y- and Z-axes are different. Along the Y-axis, the jet diverges away from the jet-axis/centerline. On the other hand, the jet converges towards the jet-axis/centerline along the Z-axis. Notice that, the generated shock wave at the corner region suppresses the expansion in the diagonal direction. Besides, there are no compression waves in the vicinity of the sidewalls; therefore, the flow turns outward along the Y-axis direction. This is due to the jet boundary on the sidewall which is pushed away from the jet axis by the closely spaced neighboring shock waves. As the nozzle pressure ratio increases to 4, the size of shock cell structures to compensate for the increasing pressure gradient both planes (Fig. 9(b)). In addition, the Mach disc begins to develop. The extent of the shock cell become larger in size when the nozzle pressure ratio is increased to 5. This is due to a stronger expansion fan at the nozzle exit at NPR 5. Basically, the jet centerline Mach number increases significantly as a result of the stronger expansion fans, which leads to shock cells of larger size. Moreover, the shock cells' number is reduced, and the Mach disk height increased at NPR 5, as shown in Fig. 9(c). The barrel shock meets the triple point and gets reflected to interact with the jet boundary.

It can be observed from the preceding discussions that both elliptic and square jets are associated with differential shock cell structures in the planes along the Y and Z axes directions. This essentially confirms the differential spreading of asymmetric jets, which eventually enhances the mixing behavior. Furthermore, at NPR 5, the Mach disc was observed for both circular and non-circular jets. Notice that, the size of the shock cells decreases continuously along the downstream distance. For the elliptic jets, the intercepting shock is noticeable along the Z-axis (minor axis). Besides, the curvature of the intercepting shock wave in an elliptic jet is substantially greater in comparison with the circular jet. On the other hand, for the square jet, the recompression shocks are prominently visible in the symmetry plane; however, the intercepting shocks are observed in both symmetry and diagonal planes.

3.2 Shock cell length

The variation of shock cell length at different nozzle pressure ratios is given in Fig. 10. The shock cell length was estimated using shadowgraph images and compared to a theoretical model. It is worth noting that the measured shock length agrees well with the theoretical model proposed by Tam
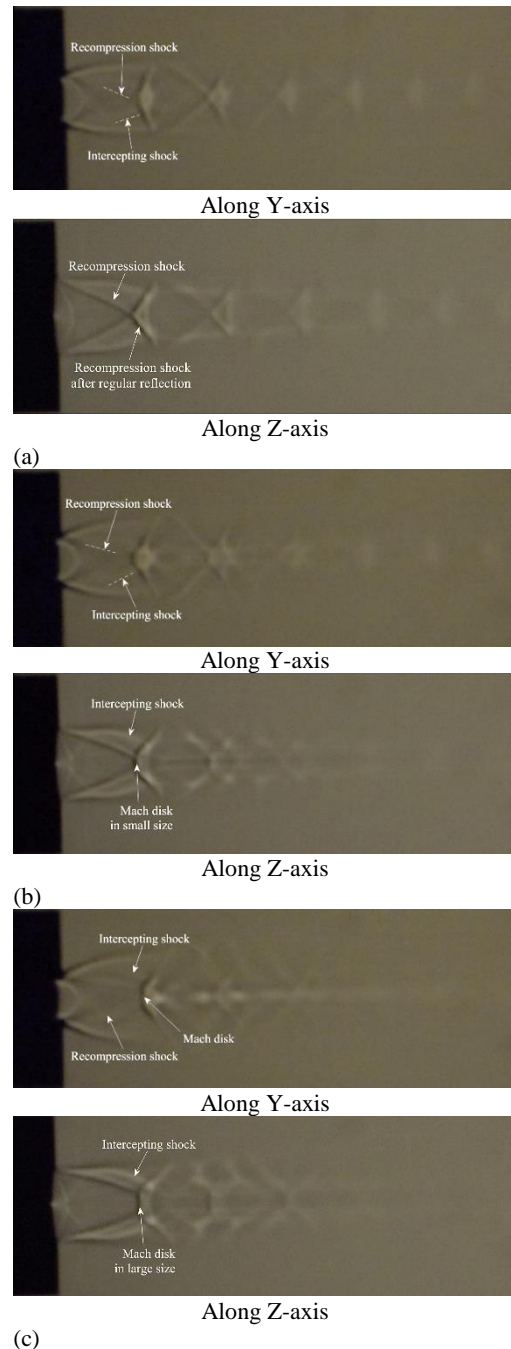

Along Y-axis

Along Z-axis

(a)

Along Y-axis

Along Z-axis

(b)

Along Y-axis

Along Z-axis

(c)

Fig. 9. Shadowgraph views of the square jet at (a) NPR 3 (b) NPR 4 (c) NPR 5.

(Tam 1988). It can be observed that, when the pressure ratio rises, the shock cell length increases. Furthermore, the second and third shock cells are shorter in length than the first shock cell. In addition, the length of the third shock cell has a relatively lesser length. The shock cells, particularly the third and fourth shock cells in the jet core, are the source of shock-associated noise in high-speed jets. The length and strength of the shock cells solely define the frequency of the screeching noise. The screech frequency is higher when the shock cell length is longer, whereas the screech frequency is lower when the shock cell length is shorter. Fig. 11 depicts the length variation
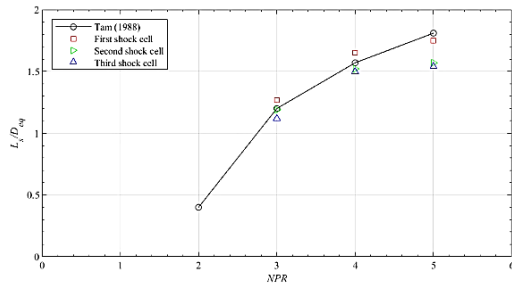
Fig. 10. Variation of shock cell length for the circular jet at different NPR.
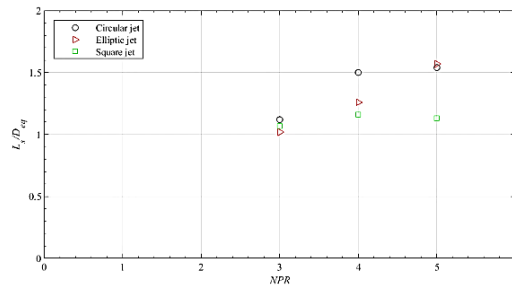

Fig. 11. Comparison of third shock cell length for various nozzle geometries at different NPR.

of the third shock cell for different nozzle geometries. In this investigation, the fourth shock cell for various nozzle geometries is either not apparent or has lost its strength. Therefore, the third shock cell was chosen for examination since it is visible in the shadowgraph images. The third shock cell length was non-dimensionalized with an equivalent nozzle diameter and plotted against the NPR. It can be noted that the shock cell length for both axisymmetric jet and asymmetric jet is almost the same for NPR 3. At NPR 3, a larger shock cell length was observed for the circular jet. When both elliptic and square jets are considered, the elliptic jet possesses the shortest shock cell length. Subsequently, the shock cell length was increased in the axisymmetric jet and asymmetric jet by increasing the NPR to 4. At NPR 4, the shock cell length of the circular jet is greater than that of the asymmetric jets. Surprisingly, at this NPR, the square jet has the shortest shock cell length. As the NPR increased to 5, the shock cell length of the elliptic and circular jets increased, whereas the shock cell length of the square jet decreased. Here, the circular and elliptic jets have almost similar values of shock cell length. The shortest shock cell length was obtained for the square jet. As the reduced shock cell length is advantageous in mitigating the shock-associated noise, the asymmetric nozzle provides the best possible solution for reducing the shock-associated noise in all the NPRs.

4. CONCLUSIONS

The experiments were carried out to investigate the shock cell structures in the underexpanded jets ejected from the circular, elliptic, and square nozzle geometries. The shadowgraph technique has been used to visualize the waves prevailing at the nozzle exit. The tests were performed at moderate and highly underexpanded levels, with corresponding pressure ratios of 3, 4, and 5. The results revealed that the incident and reflected shocks occurred at mild and moderate expansion levels in the circular jet core region. At highly underexpanded condition, the Mach disk, triple points, and slip lines were observed It can be noted that the square jet and the elliptic jet exhibit distinct shock patterns along their different plane axes. For elliptic jets, the intercepting shock is prominent along the minor axis when compared it to the major axis. The curvature of the intercepting shock for elliptic jet is greater than that of the circular jet. In addition, the size of the Mach disc is larger along the major axis. On the other hand, the square jet shows the recompression shock near the nozzle exit in the symmetry plane direction, whereas, along the diagonal direction, the recompression shock was generated at some downstream distance. Interestingly, the jet diverges along the symmetry plane but converges along the diagonal plane. Besides, the shock cell lengths predicted from shadowgraph pictures were compared to a theoretical model where the experimentally obtained results are in good agreement with the theoretical values.

REFERENCES

Adamson, T. C. and J. A. Nicholls (1959). On the Structure of Jets from Highly Underexpanded Nozzles into Still Air. *Journal of Aerospace Sciences* 26, 16–24.

Addy, A. L. (1981). Effects of axisymmetric sonic nozzle geometry on Mach disk characteristics. *AIAA Journal* 19, 121–122.

Austin, T. and C. M. Ho (1992). Controlled entrainment in a 2:1 Aspect-Ratio Subsonic Elliptic Nozzle. AIAA 92-0537, *30th Aerospace Sciences Meeting and Exhibit*, Reno, NV 1–11.

Gutmark, E. and C. M. Ho (1986). Visualization of a forced elliptic jet. *AIAA Journal* 24, 684–685.

Ho, C. M. and E. Gutmark (1987). Vortex induction and mass entrainment in a small-aspect-ratio elliptic jet. *Journal of Fluid Mechanics* 179, 383–405.

Ilakkiya, S. and B. T. N. Sridhar (2018). An experimental study on the effect of square grooves on decay characteristics of a supersonic jet from a circular nozzle. *Journal of Mechanical Science and Technology* 32, 4721–4729.

Jana, T. and M. Kaushik (2021). Performance of corrugated actuator-tabs of aspect ratio 2.0 on supersonic jet mixing enhancement. *Journal of Mechanical Science and Technology* 35, 1087–1097.

Jiang, Z., O. Onodera and K. Takayama (1999). Evolution of shock waves and the primary vortex loop discharged from a square cross-sectional tube. *Shock Waves* 9, 1–10.

Jothi, T. J. S. and K. Srinivasan (2013). Turbulent mixing noise from underexpanded non-circular slot jets. *Acta Acustica united with Acustica* 99, 514–523.

Jothi, T. J. S. and K. Srinivasan (2019). Shock structures of underexpanded non-circular slot jets. *Sādhanā* 44, 1–9.

Kaushik, M. (2019). *Theoretical and Experimental Aerodynamics*. 1st edition, Springer Nature, Singapore.

Lee, S. J., Y. G. Jang and Y. S. Choi (2012). Stereoscopic-PIV measurement of turbulent jets issuing from a sharp-edged circular nozzle with multiple triangular tabs. *Journal of Mechanical Science and Technology* 26, 2765–2771.

Menon, N. and B. W. Skews (2010). Shock wave configurations and flow structures in non-axisymmetric underexpanded sonic jets. *Shock Waves* 20, 175–190.

Mitchell, D. M., D. R. Honnery and J. Soria (2013). Near-field structure of underexpanded elliptic jets. *Experiments in Fluids* 54.

Rajakuperan, E. and M. A. Ramaswamy (1998). An experimental investigation of underexpanded jets from oval sonic nozzles. *Experiments in Fluids* 24, 291–299.

Rathakrishnan, E. (2007). *Instrumentation, Measurements, and Experiments in Fluids*. CRC Press, Boca Raton, FL.

Schadow, K. C., E. Gutmark, S. Koshigoe and K. J. Wilson (1989). Combustion-related shear-flow dynamics in elliptic supersonic jets. *AIAA Journal* 27, 1347–1353.

Tam, C. K. W. (1988). The shock-cell structures and screech tone frequencies of rectangular and non-axisymmetric supersonic jets. *Journal of Sound and Vibration* 121, 135–147.

Tanna, H. K. (1977). An experimental study of jet noise part II: Shock associated noise. *Journal of Sound and Vibration* 50, 429–444.

Thangaraj, T., M. Kaushik, D. Deb, M. Unguresan and V. Muresan (2022). Survey on Vortex Shedding Tabs as Supersonic Jet Control. *Frontiers in Physics* 9, 1–17.

Tsutsumi, S., S. Teramoto, K. Yamaguchi and T. Nagashima (2006). Structure of underexpanded jets from square nozzles. *AIAA Journal* 44, 1287–1291.

Verma, S. B. and E. Rathakrishnan (2001). Effect of Mach number on the acoustic field of 2:1 elliptic-slot jet. *The Aeronautical Journal* 105, 9–16.

Verma, S. B. and E. Rathakrishnan (1998). Mixing Enhancement and Noise Attenuation in Notched Elliptic-Slot Free Jets. *International Journal of Turbo and Jet Engines* 15, 7–25.

Zare-Behtash, H., K. Kontis and N. Gongora-Orozco (2008). Experimental investigations of compressible vortex loops. *Physics of Fluids* 20, 1–18.

Zhang, H., Z. Chen., Z. Guo and X. Sun (2017). Characteristic behavior of shock pattern and primary vortex loop of a supersonic square jet. *International Journal of Heat and Mass Transfer* 115, 347–363.